Supplemental information for "Lossless Positron Injection into a Magnetic Dipole Trap"

E. V. Stenson,* S. Nissl, U. Hergenhahn, J. Horn-Stanja, M. Singer, H. Saitoh, T. Sunn Pedersen, J. R. Danielson, M. R. Stoneking, M. Dickmann, and C. Hugenschmidt

(Dated: August 1, 2018)

Abstract

This document provides supplemental information for the manuscript "Lossless Positron Injection into a Magnetic Dipole Trap", such as additional details of the experiment and simulation set-ups, as well as complementary presentations of select results.

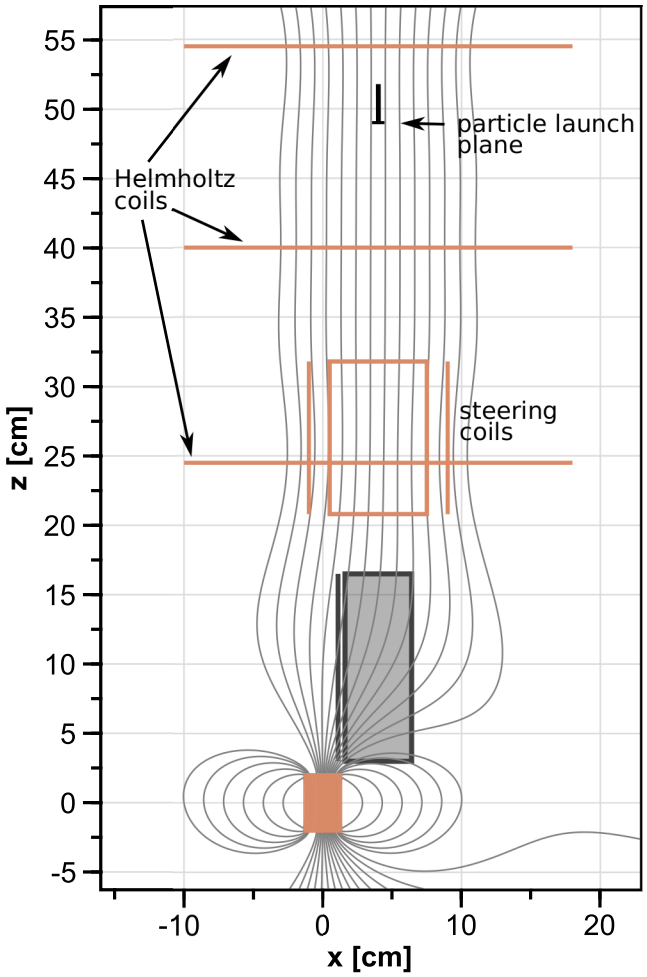

FIG. 1. AlGeoJ diagram showing the relative positions and sizes of the permanent magnet, steering coils, and Helmholtz coils, plus magnetic field lines when the steering coils are not energized ($I_r = I_\theta = 0$). The $\mathbf{E} \times \mathbf{B}$ and shield plates are also shown for reference, as is the starting height of the particle trajectories for AlGeoJ injection simulations.

Figure 1 shows the sources of the magnetic field, as illustrated in the AlGeoJ interface. The Helmholtz coils generate a 5-mT field (so as to match the NEPOMUC beam line); the field of the permanent magnet has a strength of 0.6 T at the poles. The rectangular r and θ steering coil pairs generate magnetic fields primarily in the $+x$ and $+y$ directions, respectively. (The coordinate system is right-handed, so $+y$ is into the page.) The plane from which particles were launched for AlGeoJ injection simulations was chosen to coincide with the height of the insertable beam monitor — containing a copper target plate, micro-channel plate [MCP] assembly, and apertures — that is used to center and characterize the NEPOMUC positron beam as it arrives at the open beam port. (The beam monitor

is retracted during injection experiments.) SIMION simulations used a comparable magnetic field set-up but did not consider the steering coils, and particles were launched from $z = 22$ cm. For each simulation, 50-200 particles were launched, either all from the same starting point (SIMION) or with an initial spatial spread matching measured beam parameters (AlGeoJ). Initial velocities were generated as random draws from energy and spatial distributions matching measured values (Ref. [28] of the main manuscript). Interactions between particles were not considered, as is consistent with the very low volumetric densities involved.

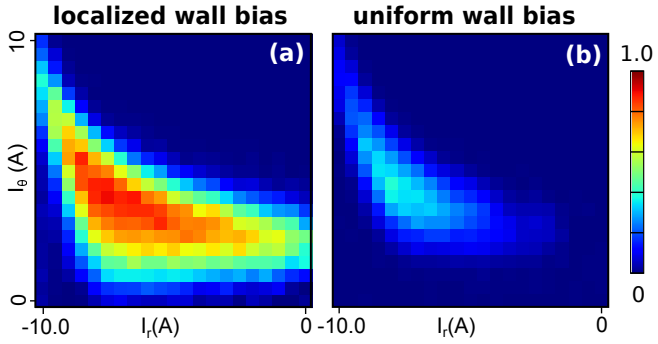

FIG. 2. Experiment data showing 2D scans of the $I_r I_\theta$ plane of the parameter space for injection with (a) top1 and rw1 biased (but the rest of the wall segments grounded) and (b) the entire wall set to the same positive bias.

Figure 2 shows the comparison between localized wall bias and uniform wall bias for a second plane in the multi-dimensional parameter space, in addition to the $I_r V_{E\times B}$ plane shown in Fig. 2 of the main manuscript. These illustrate that the reduced efficiency and smaller region of accessibility in parameter space for injection with a uniform wall bias cannot simply be attributed to a non-optimal choice of I_θ. (Note that the maximum injection efficiency in Fig. 2a is ∼85% rather than ∼100% due to the absence of magnet bias. Positively biasing the magnet increases injection efficiency and can shift the spatial profile of injected positrons but has little effect on the location of the peak in $I_r I_\theta$.) That the optimal value of I_θ may be nonzero in the experiment — as is the case for this data set — is attributable to imperfect alignment and/or stray magnetic fields in the part of the set-up coupling the trap to the beam line, as a result of which a beam centered on the MCP (at $z = 48$ cm in Fig. 1) may not be centered between the $\mathbf{E}\times\mathbf{B}$ plates when it arrives at $z = 17$ cm. Simulations demonstrate that in an ideal set-up (perfectly aligned beam and perfectly

aligned coils), peak injection efficiency is indeed found around $I_\theta = 0$, as one might expect. Hence, the initial position of the beam in the simulation is used as an adjustable parameter for matching the synthetic diagnostic to experimental data (as detailed in Ref. [34] of the main manuscript).

Furthermore, we have established how much the peak in $I_r I_\theta$ moves when the position of the incoming beam changes as a result of external factors affecting the upstream NEPOMUC beam line (as measured with the MCP at the Helmholtz coils). Experimental measurements and simulations are in agreement that a shift of $\sim$0.3 cm in xy corresponds to a shift of $\sim$1 A in $I_r I_\theta$ space. Combined with the fact that the peak in Fig. 2a is several amperes in each dimension, we expect high injection efficiencies to be achievable even for beams with significantly larger spatial spreads. (E.g., NEPOMUC's primary beam has at the open beam port a FWHM $\sim$5 times that of the remoderated beam and 5 to 10 times as much positron flux, as per Ref. 28 of the main manuscript.)

In color plots of 2D parameter scans, the color scale indicates the fraction of the beam that has reached the target probe. In experiments, this was determined from the number of annihilation gamma ray counts detected from the target probe region by a collimated scintillator detector. Counts detected when the target probe was fully retracted (through the outer wall, with the inner edge of the probe located 9.3 cm from the center of the trap) were subtracted from counts detected when the probe was fully inserted (with the inner edge of the probe located 5 mm from the outer surface of the magnet — i.e., at a distance of 2.2 cm from the center of the trap), thereby giving a relative measure of positrons that annihilate either on the 1-cm$\times$1-cm target or on the 3-mm-diameter rod at the end of which the target is mounted (as illustrated in Fig. 1a of the main manuscript) and to which it is electrically connected. Counts were correlated to positron flux based on measurements taken with the charge-integrating amplifier connected to the probe. These were in turn normalized to the total beam current measured at the insertable beam monitor between the Helmholtz coils (measured with the charge-integrating amplifier connected to a copper target plate). This approach was first described in Ref. [23], along with additional information about typical scintillation detection set-ups used in the experiment.

Several different approaches were investigated for generating synthetic diagnostic data from particle trajectory simulations, including:

- A particle was "detected" if it reached the $y = 0$ plane on the far side the trap from

the injection region (after having drifted toroidally ∼180° around the magnet).

- A particle was "detected" if its orbit brought it in contact with the surface of the target probe or rod. However, the calculation of the electrostatic potential in the trap did not take into account the presence of this grounded element.

- A particle was "detected" if its orbit brought it in contact with the surface of the target probe or rod, and electrostatic effects of the grounded target probe were explictly included in electric fields used to calculate particle trajectories.

For $\sim$ 5-eV positrons, differences between these approaches were found to be small.

Both the experiment and the synthetic diagnostic set-ups can produce integrated spatial profiles of positrons' locations in the trap (Fig. 3 in the main manuscript). Fitting an error function

$$f(r) = \frac{h}{2}\left(1 + \mathrm{erf}\left(\frac{r - r_{\mathrm{mean}}}{\sigma}\right)\right) \tag{1}$$

to these points yields three parameters (mean radius r_{mean}, radial spread σ, and height h) that describe the spatial distribution of positrons at the target probe, as shown in Fig. 3 above. For both injection conditions (localized injection and injection with uniform wall bias), spatial profiles obtained in three different ways — with the charge-integrating amplifier, with the scintillator detector, and from the synthetic diagnostic — produced the same r_{mean} within a few mm.

In Fig. 4, the particle trajectories shown in Fig. 6d of the main manuscript are replotted on separate axes, to facilitate more detailed examination.

Finally, Table I contains a full accounting of electrode and steering coil settings for the plots presented in this work.

---

* E-Mail: evs@ipp.mpg.de

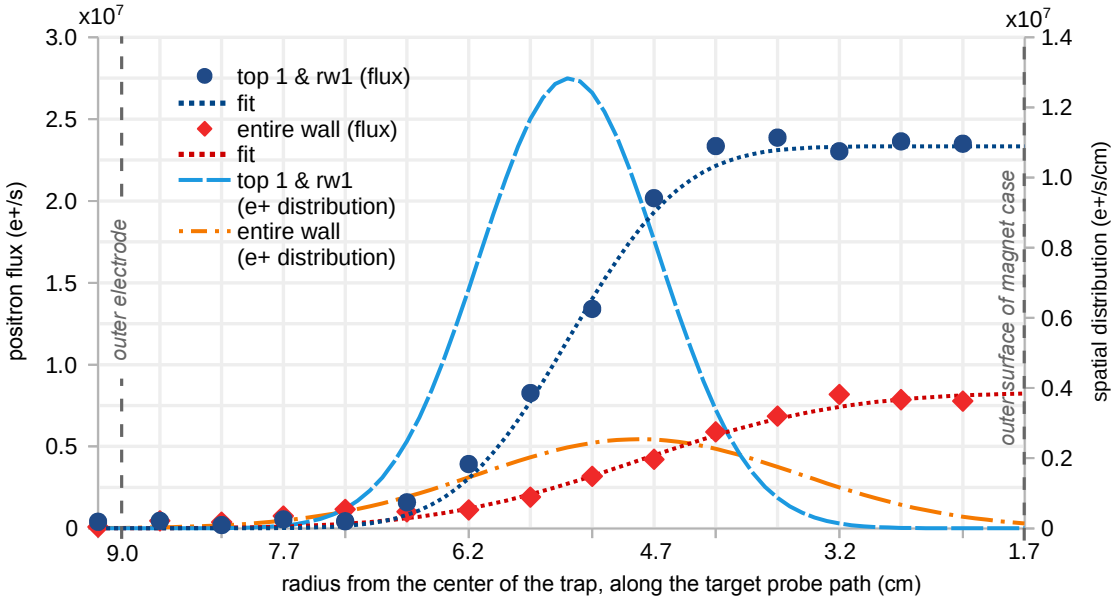

FIG. 3. Two spatial profiles from Fig. 3 of the main manuscript are fitted with error functions (dotted lines). The derivatives of these fits (dashed lines) are plotted on the secondary (right) vertical axis. The fitting parameters were $r_{\mathrm{mean}} = 5.4$ cm, $\sigma = 1.0$ cm, and $h = 2.33 \times 10^7$ e$^+$/s for the profile measured with the lossess injection condition (circles) and $r_{\mathrm{mean}} = 4.9$ cm, $\sigma = 1.8$ cm, and $h = 8.30 \times 10^6$ e$^+$/s for the profile measured with the uniform wall bias injection condition (diamonds).

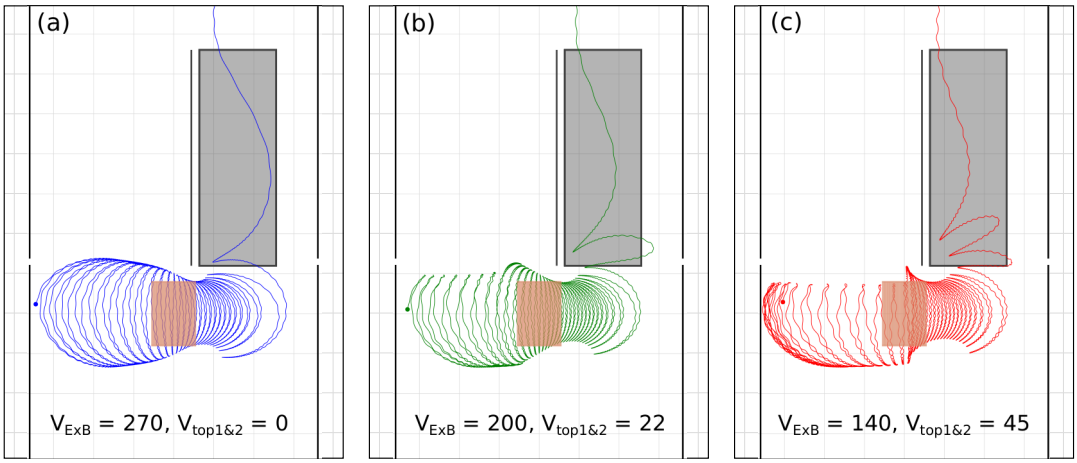

FIG. 4. Three particle trajectories, one from each of the first three islands in the $V_{E\times B}V_{top1\&2}$ parameter scan (Fig. 6 in the main manuscript). Each island corresponds to particles entering the confinement region after a different integer number m of magnetic mirroring events (alternating with reflections off the biased upper wall electrode top1, when $m > 1$).

Figure	I_R (A)	I_θ (A)	$V_{E\times B}$ (V)	V_{magnet} (V)	V_{top1} (V)	V_{top2} (V)	V_{rw1} (V)	$V_{\text{rw2-8}}$ (V)	r_{probe} (cm)
1b	N/A	N/A	220	8	14	0	20	0	N/A
2a	[-10, 0]	4	[0, 400]	8	14	0	20	0	2.2, 9.2
2b	[-10, 0]	4.5	[0, 400]	-15	7	7	7	7	2.2, 9.2
2c	[-10, 0]	4	[0, 400]	8	14	0	20	0	2.2
2d	[-10, 0]	4.5	[0, 400]	-15	7	7	7	7	2.2
3 (top1 & rw1)	-8.3	4	220	8	14	0	20	0	[2.2,9.2]
3 (entire wall)	-9	4	260	-15	7	7	7	7	[2.2,9.2]
4a	[-10, 0]	4	[0, 400]	8	22	0	0	0	2.2, 9.2
4b	[-10, 0]	4	[0, 400]	0	0	0	0	0	2.2, 9.2
4c	[-10, 0]	4	[0, 400]	8	22	0	0	0	2.2
4d	[-10, 0]	4	[0, 400]	0	0	0	0	0	2.2
5a	N/A	N/A	220	8	14	0	20	0	N/A
5b	N/A	N/A	175	-15	5.5	5.5	5.5	5.5	N/A
5c	N/A	N/A	0	0	0	0	0	0	N/A
6a	-8.5	6.0	[60, 400]	8	[0,40]	[0,40]	0	0	2.2, 9.2
6b	-8.5	6.0	[60, 400]	8	[0,40]	[0,40]	14	0	2.2, 9.2
6c	-8.5	6.0	[60, 400]	8	[0,40]	[0,40]	0	0	2.2
S.I., 2a	[-10, 0]	[0, 10]	180	0	12	0	12	0	2.2, 9.2
S.I., 2b	[-10, 0]	[0, 10]	180	-15	7	7	7	7	2.2, 9.2

TABLE I. Experiment/simulation settings for plots presented in this work. Square brackets indicate the maximum and minimum of a set of scanned values. Simulations that did not use steering coils or that did not explicitly simulate the target probe position are labeled N/A ("not applicable") for those values.